THE JOURNAL OF PHYSICAL CHEMISTRY B

ARTICLE

pubs.acs.org/JPCB

Multiscale Investigation of the Poly(*N*-vinylcarbazole) Photoageing Mechanism

Pierre-Olivier Bussière,[*,†,‡] Agnes Rivaton,[†,§] Sandrine Thérias,[†,§] and Jean-Luc Gardette[†,§]

[†]Clermont Université, Université Blaise Pascal, Laboratoire de Photochimie Moléculaire et Macromoléculaire, BP 10448, F-63000 Clermont-Ferrand, France

[‡]Clermont Université, ENSCCF, Laboratoire de Photochimie Moléculaire et Macromoléculaire, BP 10448, F-63000 Clermont-Ferrand, France

[§]CNRS, UMR 6505, LPMM, F-63173 Aubière, France

ABSTRACT: During the past decade, the development of polymeric solar cells has received a great deal of attention from both academic and industrial laboratories. In order to enhance the device performances both in terms of power conversion efficiency stability in use conditions, Polycarbazole copolymers have attracted increasing attention. In this paper, the photodegradation of poly(*N*-vinylcarbazole) (PVK) was investigated from the molecular scale to the nanomechanical properties. It was shown irradiation provoked chain scissions, homolysis of the C−N bond and formation of new covalent bonds between the macromolecular chains. To fully understand the mechanism of the degradation of PVK provoked by exposure to UV radiation, mechanical analyses were performed. The consequences of the cross-linking reactions on the surface modifications were analyzed. Roughness and stiffness measurements were obtained through surface analysis and nanoindentation by atomic force microscopy (AFM), and depth-profiling experiments were also performed. The surface modifications and the shape of the profiles of the degradation photoproducts were explained in light of the chemical modifications of the PVK structure. Quantitative correlations were successfully obtained between the main relevant criteria of degradation, from the chemical structure to the mechanical properties. It was found that cross-linking reactions were prevalent.

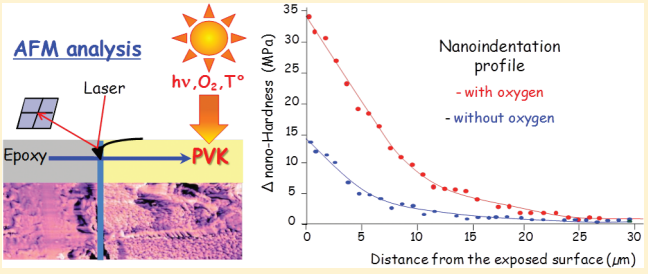

1. INTRODUCTION

To resolve the problem of the exhausting of fossil energy sources such as petroleum and coal, different strategies are attempted to develop new renewable energy sources, or convert one kind of energy to another convenient style, among which, the solar energy is, perhaps, the most promising one. For this purpose, the development of polymeric solar cells[1−8] has received a great deal of attention from both academic and industrial laboratories. Organic solar cells (OSCs), commonly based on an active layer made of a blend film of conjugated polymer donor such as poly(3-hexylthiophene) (P3HT) and fullerene derivative acceptor have been extensively studied over the last years. Several studies have focused on the stability of the polymers used to form these active layers, which are known to be sensitive to the aging provoked by light, temperature, oxygen and water. Along these lines, polycarbazole copolymers could be promising candidates because they are known to be more stable in air and capable of withstanding high temperatures for extended periods of time.[9−11] We decided to focus our work on poly(*N*-vinylcarbazole) (PVK) and to study the degradation of this polymer caused by exposure to light in the presence and in absence of oxygen .

The photoaging of PVK (Figure 1) has recently been studied,[12,13] and its photodegradation mechanism has been shown to be governed by chain-scission and cross-linking reactions.[13,14]

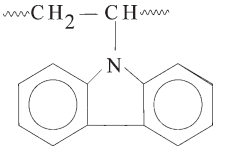

Figure 1. Structure of PVK.

The proposed photoaging mechanism[12] indicates that light absorption ($\lambda > 300$ nm) provokes the homolysis of C−N bonds on the macromolecular chains, which forms a carbazolyl radical and a macroradical on the polymeric chain. The macroradical might recombine, leading to cross-links that can include oxygen atoms.[15] The carbazolyl radical is likely to initiate chain oxidation by hydrogen abstraction on the macromolecular chains.[16] The abstraction of a hydrogen atom occurs preferentially at the tertiary carbon of the structure, leading to a polycarbazolyl radical. The polycarbazolyl radical can also react with oxygen to give hydroperoxide, which decomposes to give an alkoxy radical. Several reactions are then likely to occur, the main being

Received: November 25, 2011
Revised: December 19, 2011
Published: December 19, 2011

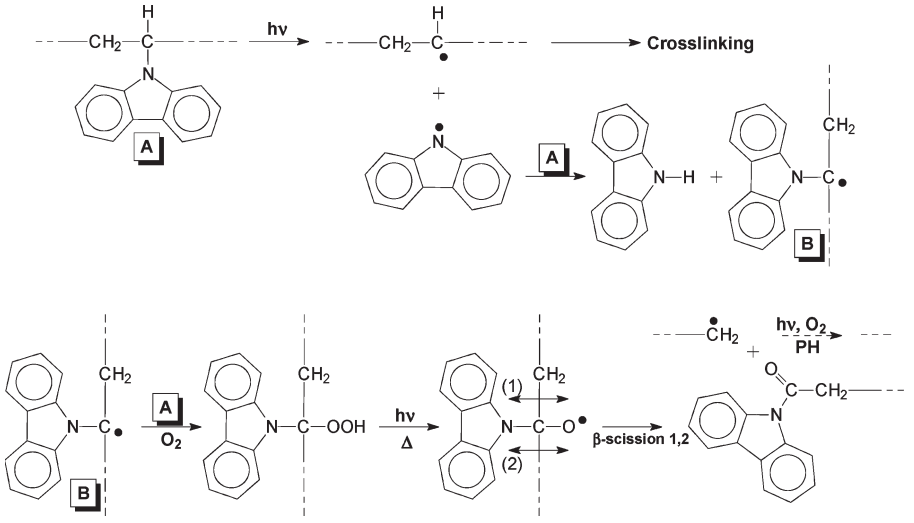

Figure 2. Degradation mechanism of PVK.

identified as the β-scission of this alkoxy radical, which gives an *N*-acetylcarbazole group. This last reaction is accompanied by the formation of an alkyl radical that can be oxidized to carboxylic acid or that can isomerize to a more stable tertiary radical. This last radical continues the oxidation process leading to chain scissions. It is important to note that this mechanism, represented in Figure 2, indicates the predominance of the chain-scission reaction versus the cross-linking reaction.

PVK is a thermoplastic polymer made of linear macromolecular chains. The progressive formation under irradiation of a three-dimensional network due to cross-linking reactions is expected to generate modifications of the mechanical properties of the material. As a consequence, the photodegradation process needs to be investigated at different levels of analysis. In the literature,[17−20] the degradation of polymers has been, for the most part, analyzed at the molecular scale by spectroscopic techniques that permit the characterization of reactions involving oxygen fixation and rearrangements. Chromatographic methods, such as size exclusion chromatography (SEC), also give molecular information on the modifications of the molecular weight during irradiation. Gel fraction analysis and swelling of films irradiated in the presence of oxygen revealed an increased amount of the insoluble fraction. However, the information given by this technique depends on the nature of the solvent used for the test, and no quantitative information can be obtained when insolubility reaches 100%.[14]

The recent use of atomic force microscopy (AFM) has demonstrated that this technique is a powerful tool[8−11] to monitor the polymer surface modifications due to aging has demonstrated that this technique is a powerful tool.[21−24] Topographic information as well as nanomechanical properties can be obtained by AFM. The nanomechanical properties, such as stiffness, elastic modulus and hardness can be determined from indentations curves realized with the AFM tip. In a previous paper,[25] we have shown that the AFM indentation mode can also be used to realize depth profiling at a nanometric level.

The aim of this paper is to give evidence of the consequences of photochemical reactions on the macroscopic properties of a polymer such as PVK and to qualitatively and quantitatively confirm the direct relationship between the modifications of the chemical structure and the modifications of the mechanical properties.

2. EXPERIMENTAL SECTION

2.1. Samples. Free-standing thin (5−15 μm) and thick (100 μm) films of PVK, (M_w = 1 100 000, T_g = 501 K, Aldrich, Germany) were prepared by evaporation of polymer solutions in 1−4 dioxane. Before profile measurements, the irradiated samples were embedded in an epoxy resin and then microtomed. The obtained slices were analyzed by micro-FTIR and by AFM from the irradiated surface to the core of the sample.

2.2. Photo-Oxidation and Photolysis. Irradiation was performed under artificial aging conditions. The aging device used was a SEPAP 12/24 unit[26] from Atlas, equipped with four medium-pressure mercury lamps (Novalamp RVC 400 W) located in a vertical position at each corner of the chamber. Wavelengths less than 295 nm were filtered by the glass envelope of the sources. The temperature at the surface of the samples was fixed at 60 °C. Photolysis experiments were performed on samples that were introduced in borosilicate tubes which were sealed under very low pressure (10^{-3} Pa) using a diffusion vacuum line. The tubes were then placed in the SEPAP 12/24 device.

2.3. Analysis. The cross-linking of the polymer at the macroscopic scale was evaluated by gravimetric measurements of the gel fraction (Gf). The irradiated films (approximately 10 mg) were immersed in tetrahydrofuran (THF, 10 mL) for 48 h. The solutions were then Büchner filtered. The insoluble fractions were dried in an oven at 100 °C and then weighed. Thus, it is possible to determine the polymer insoluble part (Gf), which corresponds to the proportion of cross-links. Gf can be expressed by eq 1

$$\mathrm{Gf} = \frac{M_{\mathrm{insoluble}}}{M_{\mathrm{initial}}} \qquad (1)$$

The average molecular weights (M_w) of the polymeric samples were obtained by Size Exclusion Chromatography (SEC) using an universal calibration. SEC was carried out on a VISCOTEK Trisec 270 Controller using a viscotek viscosimetric detector. The mobile phase was either THF or CH_2Cl_2 (HPLC grade) separated in a GMH_{xl} column at a flow rate of 1 mL.min^{-1}. The calibration was performed using polystyrene standards.

The chemical changes caused by oxidation reactions were determined by infrared spectrometry (IR spectroscopy). For each

dx.doi.org/10.1021/jp211358q | J. Phys. Chem. B 2012, 116, 802–812

irradiation time, IR spectra were recorded using a Nicolet FTIR 760 spectrophotometer (nominal resolution of 4 cm^{-1}, 32 scans summation). This apparatus is equipped with a Continuum microscope allowing micro-FTIR measurements (sample thickness: 30 to 100 μm, displacement: 5 or 6.5 μm, window width: 10 to 15 μm, number of scans: 128, resolution: 4 cm^{-1}).

Vickers micro-hardness (Hv) measurements were performed on a Shimadzu hardness tester. Hv can be expressed by eq 2

$$\mathrm{Hv} = 1.8544 \times 10^6 \frac{P}{d^2} \tag{2}$$

where P is the applied load in N and d is the diagonal of the indentation in mm. Hv is expressed in MPa. In the present study, P was fixed at 0.343 N, and the application time was 10 s.

The glass transition temperature of the polymer was measured with a Mettler Toledo DSC 822 programmed from 10 to 350 °C at a heating rate of 15 °C min^{-1}. Analyses were performed on films with thickness of less than 20 μm that had been placed in a 40-μL crucible.

A Nanoscope IIIa atomic force microscope (AFM) from Veeco Instruments was used for surface topography measurements and nanoindentation. Imaging was achieved using the repulsive mode in intermittent contact, more commonly called "tapping" mode. After various durations of photoaging, images of 10 μm × 10 μm were recorded. The rms (root mean square) was determined on zooms of 5 μm × 5 μm. The rms or roughness represents the standard deviation of the Z-axis values of a given surface. The rms is obtained by a computer-aided calculation on the entire surface studied via the following mathematical eq 3

$$\mathrm{RMS} = R_q = \sqrt{\frac{\sum (Z_i - Z_{ave})^2}{N}} \tag{3}$$

Z_{ave} is the average value in Z, Z_i is the considered value, and N is the total numbers of points.

The evolution of the mechanical properties versus irradiation time was determined using AFM nanoindentation. The force−distance curves were monitored under a constant deflection (or constant load). Nanoindentations were performed using a diamond tip (64.05 kHz). The given characteristics of the diamond tip correspond to a spring constant of 204.5 N m^{-1} and a radius of curvature of 25 nm. To determine the relative stiffness of the polymer, three nanoindentation tests in different areas of the polymer were performed. Each test corresponds to nine indentations; thus, 3 × 9 force curves were used with a load variation from 1 to 5 μN. In the literature, several models[27−29] have been proposed to measure the mechanical properties from the nanoindentation testing method. One of these models is the Oliver and Pharr (OP) procedure.[30] This procedure was first used with commercial nanoindenters and then applied in previous works[31] to measure the hardness and Young's modulus of polymers analyzed by AFM nanoindentation.

Thus, the data extracted from the force-displacement curve obtained with AFM nanoindentation measurements have been used according to the model proposed by OP. The OP procedure is based on Sneddon's[32] approach, in which the force F is given as a power law of displacement, $F(h) = \alpha h^m$, where α and m are constants that depend on the mechanical properties of the polymer and indenter geometry, respectively. The model assumes that the sample deformation is elastic and plastic, deformation is time-independent, the indenter is a rigid punch and there is no sink-in or pile-up. Figure 3 gives an illustration of the OP procedure.

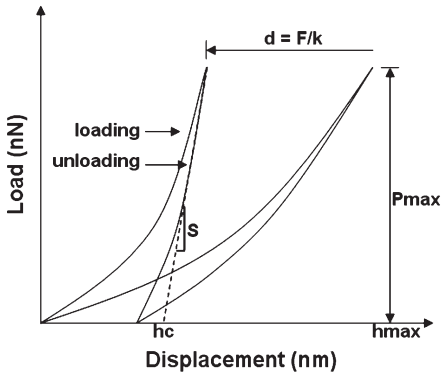

Figure 3. Schematic illustration of the force-displacement curve. The meaning of the parameters is described in the text.

The hardness is defined by eq 4 and the reduced elastic modulus is given in eq 5

$$H = \frac{F_{max}(h_{max})}{a(h_c)} \tag{4}$$

$$E = \frac{S}{2\beta}\sqrt{\frac{\pi}{A(h_c)}} \tag{5}$$

where S is the slope of the unloading curve and β = 1.034 for a Berkovitch indenter. Modulus was obtained from the unloading curve of indentation because during the loading of a sample elastic−plastic deformation occurs, while the initial unloading is an elastic event. The initial slope of the unloading curve (called stiffness) can therefore be used to calculate the reduced Young's modulus of the sample.[33−36]

If h_c is known, then the area function can be calculated.

$$A(h_c) = 24.56 h_c^2 \tag{6}$$

It should be noted that AFM nanoindentation is different from conventional nanoindentation because the former implies a cantilever deflection

$$F(d) = kd \tag{7}$$

where k is the cantilever stiffness and d is the cantilever deflection. Assuming this, the raw data, that is, the force-displacement ($F-z$) curve, are converted to a force−indentation ($F-h$) curve. The indentation depth is given by eq 8

$$h = z - d \tag{8}$$

where z is the piezoelectric displacement and d is the cantilever deflection. The conversion of the $F-z$ curve to the $F-h$ curve is depicted in detail in Figure 3.

The elastic modulus (E) could be directly calculated from the reduced modulus given previously, but a quantitative determination (i.e., elastic modulus) required a well-characterized tip (spring constant, curvature radius, etc.). The AFM displacements also needed to be calibrated, and the piezoelectric hysteresis had to be accounted for. When all of these requirements were met, the obtained data still contained a rather large uncertainty.[31] As a consequence, the stiffness variation corresponding to the nanohardness (nano-H, expressed in MPa) that will be proposed in the next section should be considered as a versatile tool to measure the mechanical properties of polymers. This means that

dx.doi.org/10.1021/jp211358q | J. Phys. Chem. B 2012, 116, 802–812

the absolute value of calculated modulus as to be taken with caution and that is the reason why we will concentrate on comparing modulus evolutions during aging.

3. RESULTS AND DISCUSSION

A. Irradiation in the Absence of Oxygen. *3.A.1. Modifications of the Chemical Structure As Measured by SEC, Gel Fraction, and FTIR.* To complete the results given in a previous paper,[12,14] we determined the amount of insoluble fraction and the molecular weight (M_w) of the soluble part for increasing irradiation time. The obtained results for different exposure times in the absence of oxygen (photolysis) are reported in Table 1.

The results given in Table 1 show that, when irradiation is performed in the absence of oxygen, nearly total insolubility of the polymer is obtained after 20 h of irradiation and that the maximum value of M_w is reached after 3 h of exposure. These results indicate that cross-linking is the main phenomenon occurring during the initial irradiation period of PVK films.

Table 1. Evolution of the Molecular Weight and Gel Fraction with the Irradiation Time in the Absence of Oxygen

time (h)	M_w ($\times 10^3$)	Gf (%)
0	1100 ± 190	0
1	2120 ± 110	40
3	2700 ± 260	50
6	2090 ± 100	55
12	1230 ± 80	70
15	900 ± 120	70
20	540 ± 90	75

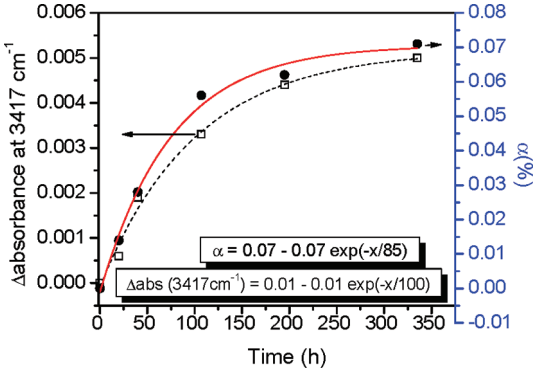

Figure 4. Conversion rate of the C−N groups at 1224 cm^{-1} (●) and Δabsorbance at 3417 cm^{-1} (□) versus photoaging in the absence of oxygen. The circles and square represent the experimental points and the line is a kinetic curve obtained by an exponential fit.

Photolysis in the absence of oxygen in PVK also provokes modifications in the IR and UV−visible spectra. The main modifications of the chemical structure were revealed by IR analysis[1] mostly in two domains of the spectrum between 2700 and 3700 cm^{-1}, respectively corresponding to the CH and NH/OH groups and in the fingerprint domain (600−1300 cm^{-1}).

- In the region between 2700−3700 cm^{-1}, the formation of a new absorption band at 3417 cm^{-1} was observed upon exposure. In a previous paper,[1] this band was attributed to the ν(N−H) vibration of molecular, "free" carbazole, which reflects scissions of the N−C bond.
- In the region between 600 and 1300 cm^{-1}, several modifications were noticed. The main feature was the disappearance of the band at 1224 cm^{-1}corresponding to the C−N bond, which is actually a bond between the macromolecular chain and the pendant carbazole unit.

The decrease of absorbance at 1224 cm^{-1} (corresponding to the C−N bond) is represented by the conversion rate α, and the increase of absorbance at 3417 cm^{-1} (corresponding to the formation of the N−H bond) are compared in Figure 4 (the relative conversion α used for the 1224 cm^{-1} band is defined by eq 9).

$$a = (C_0 - C_t)/C_0 \quad (9)$$

The two curves reported in Figure 4 confirm that the scission of the pendant N−C bond and the release of molecular carbazole are two linked phenomena. One observes that the IR band at 3417 cm^{-1} and the relative conversion α used for the 1224 cm^{-1} increase linearly under irradiation with a change in the slope and a slower rate after approximately 100 h of exposure.

3.A.2. Modifications of the Physical Properties. ***a. Surface.*** AFM measurements in nanoindentation mode were performed. Figure 5 shows the loading/unloading indentation curves for two irradiation times.

The data reported in Figure 5 show a weak slope in the case of the nonirradiated sample whereas a higher slope with an important decrease in the hysteresis was obtained in the case of the sample irradiated for the longest duration (500 h). These data are characteristic of an increase in the surface Hv and Young's modulus, which are consistent with the observations reported above. Quantitative values of these properties can be estimated

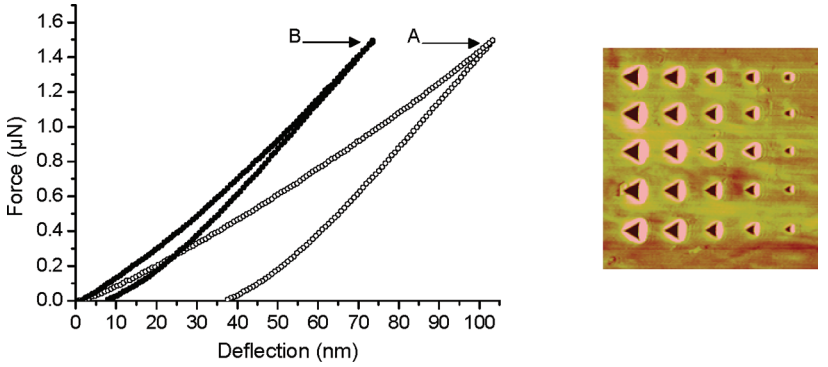

Figure 5. Left: force-displacement curves of PVK at different irradiation times. Trace A, unaged; trace B, aged 500 h. Right: image of the AFM nanoindentations on the PVK surface.

dx.doi.org/10.1021/jp211358q | J. Phys. Chem. B 2012, 116, 802–812

by various mathematical models. We used the OP[30] procedure to calculate theoretical values of the nano-H. Figure 6 gives the obtained values of the Δnano-H as a function of irradiation time.

The results reported in Figure 6 indicate that the stiffness increased under irradiation with a slope change and a lower rate after ∼100 h of exposure in the absence of oxygen. The increase in absorbance at 3417 cm^{-1} is shown in the same figure. The shapes of the curves are very similar. These results highlight the close relationship between the modifications of chemical structure and those of the mechanical properties provoked by light irradiation in the absence of oxygen.

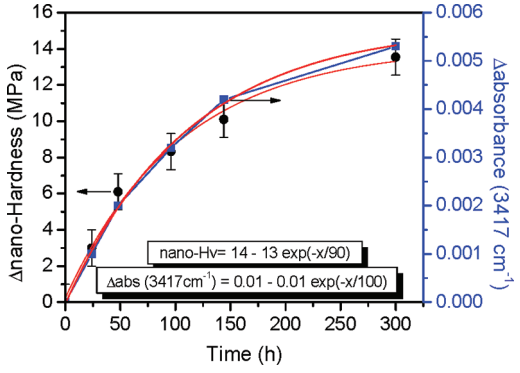

Figure 6. Δnano-H (●) and Δabsorbance at 3417 cm^{-1} (■) versus photoaging in the absence of oxygen. The circles and square represent the experimental points, and the line is a kinetic curve obtained by an exponential fit.

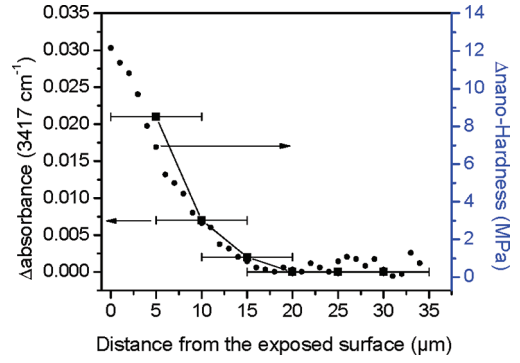

Figure 7. Δnano-H (●) and Δabsorbance at 3417 cm^{-1} (■) versus distance from the exposed surface of a polymer film irradiated for 200 h in the absence of oxygen.

b. Degradation Profile. To evaluate the cross-linking rate within the thickness of the irradiated films, depth profiling was performed by AFM in nanoindentation mode. The stiffness profiles were obtained for PVK films with a thickness of approximately 100 μm, the nanoindentations curves being recorded every micrometer. The stiffness variations versus the distance from the exposed surface after 200 h of exposure are presented in Figure 7. The same figures are reported in the cross-sectional analysis by IR microspectroscopy that characterizes the distribution of the free carbazole molecular formed and thus the C−N bond cleavage within the exposed sample thickness.

One can observe that the stiffness increases and the formation of the free carbazole inside the polymer matrix were heterogeneously distributed and that the profiles were very similar in terms of thickness of the degraded zone, approximately 25 μm. This experiment confirmed that the formation of the carbazolic free groups and the stiffness were linked. The modifications resulting from photolysis only result from rearrangements and cross-linking reactions. Those reactions are controlled by the light penetration into the polymer, and the profiles shown in Figure 7 fit perfectly the light absorption profile, as calculated from the Beer−Lambert law ($A = \varepsilon cl$) and reported in Figure 8.

3.A.3. Mechanism of Degradation. On the basis of this first set of results, we can propose a mechanism of degradation of PVK in the absence of oxygen. Irradiation of PVK provokes scission of the N−C bond, which gives a carbazolyl radical (B) and a macroalkyl radical. These radicals have already been identified by ESR spectroscopy.[37] Abstraction of hydrogen by the carbazolyl radical (B) leads to the formation of molecular carbazole that is trapped in the irradiated film and characterized by an IR band at 3417 cm^{-1} of N−H bond. Abstraction of a hydrogen atom preferentially occurs on tertiary carbon atoms of the macromolecular chains structure, leading to a polycarbazolyl radical (D). These radicals (D and macroalkyl) formed simultaneously might recombine, leading to cross-linking. As it can be noticed in the proposed mechanism (Figure 9), the more carbazolyl radicals (B) that are produced, the more important the cross-linking reaction is. A direct relationship exists between photoproducts B, D and the macroalkyl radical, which is confirmed by the experimental results reported above.

B. Irradiation in the Presence of Oxygen. *3.B.1. Modifications of the Chemical Structure As Measured by SEC, Gel Fraction, and FTIR.* In the case of irradiation in the presence of oxygen (photo-oxidation), the evolutions of molecular weight M_w of the irradiated PVK films were also monitored and the obtained results are reported in Table 2. One can see that the M_w increased

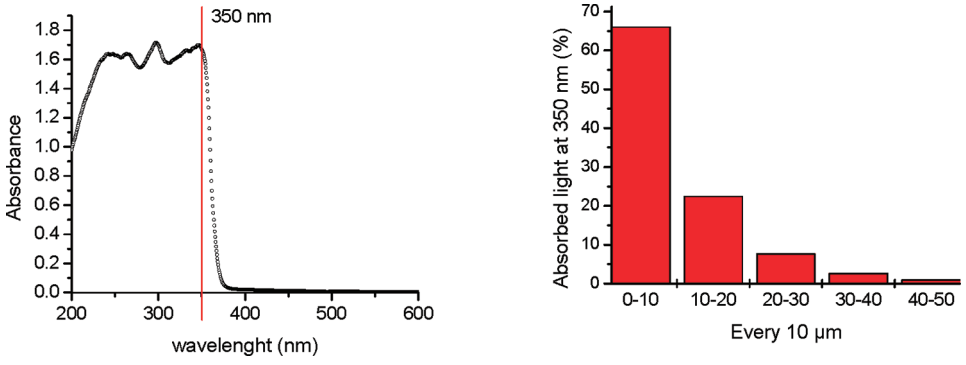

Figure 8. Left: UV−visible spectrum of a pristine PVK sample (thickness 50 μm). Right: % of absorbed light at 350 nm versus distance (μm) for a pristine PVK film.

dx.doi.org/10.1021/jp211358q | J. Phys. Chem. B 2012, 116, 802–812

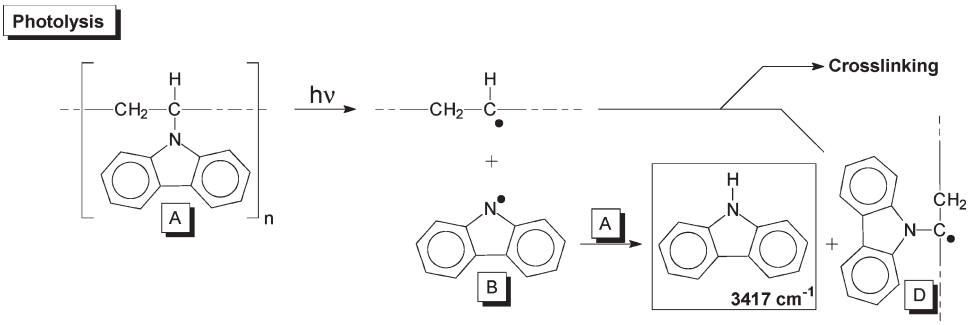

Figure 9. Photolysis mechanism of PVK.

Table 2. Evolution of the Molecular Weight and Gel Fraction with the Irradiation Time in the Presence of Oxygen

time (h)	M_w ($\times 10^3$)	Gf (%)
0	1100 ± 190	0
0.1	3150 ± 440	25
0.5	3350 ± 210	40
1	1930 ± 50	65
2	1100 ± 350	80
3	690 ± 150	85
5	270 ± 90	95

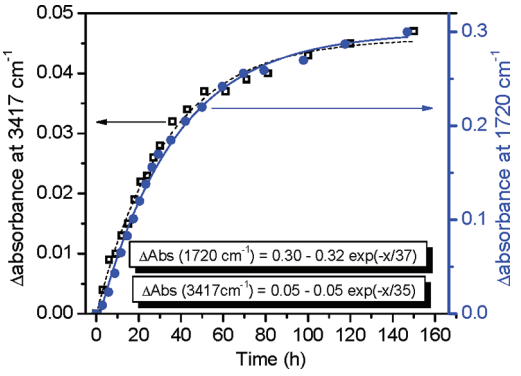

Figure 10. Δabsorbance at 1720 cm^{-1} (●) and at 3417 cm^{-1} (□) versus photo-oxidation duration. Circles and square represent the experimental points, and the lines are the extrapolated curves obtained by an exponential fit.

under exposure and reached a maximum value (3 300 000) after only 0.5 h of irradiation. Then, an insoluble network was formed, and M_w rapidly decreased, reaching a very low value, which reflected that only oligomerics were soluble in THF. Moreover, these results indicate that, for the same irradiation time, M_w and Gf are higher for irradiation performed in the presence of oxygen.

The main modifications of the chemical structure can be characterized by IR spectroscopy. Most of the modifications occurred in three parts of the spectrum: the hydroxyl (2700−3700 cm^{-1}), carbonyl (1400−1900 cm^{-1}) and fingerprint regions (600−1300 cm^{-1}).

- In the region between 2700−3700 cm^{-1}, the formation of a broad band between 3100 and 3600 cm^{-1} was observed. Three absorption maxima were observed after subtraction of the spectrum recorded before irradiation, at 3525, 3417, and 3260 cm^{-1}. These maxima were ascribed to the formation of OH, NH, and COOH end groups, respectively,[1] which result from oxidation of the polymer, accompanied by a decrease in the CH bands.
- In the region between 1400 and 1900 cm^{-1}, the formation of a CO band with a maximum centered at 1720 cm^{-1} was noticed. This band was attributed by chemical derivation[20] to anhydrides, acid groups and to a ketone, that was quantitatively identified as the main photoproducts.
- In the region between 600 and 1300 cm^{-1}, several modifications were noticed. The main feature was the decrease of absorbance at 1224 cm^{-1} corresponding to the loss of C−N bond.

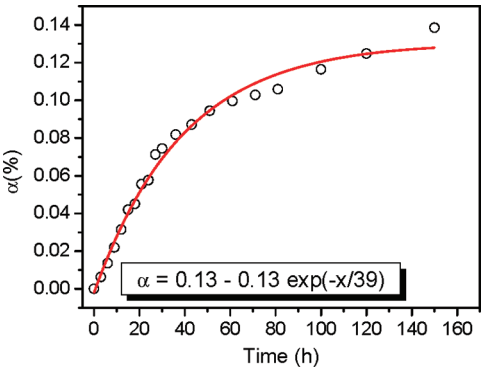

Figure 11. Conversion rate of the C−N groups at 1224 cm^{-1} versus photo-oxidation duration. The circles represent the experimental points and the line is a kinetic curve obtained by an exponential fit.

Photo-oxidation of PVK can be followed by an increase in the carbonyl (i.e., ketone) and NH groups at 3417 and 1720 cm^{-1}, respectively. The absorbance at 1720 and 3417 cm^{-1} were plotted as a function of irradiation time, and the obtained curves are shown in Figure 10.

As shown in Figure 10, the curves are characterized by two periods: the first with a rapid increase within 50 h of exposure and the second with a lower rate. As demonstrated in the previous discussion, the scission of C−N bonds could be followed by a decrease in the intensity of the band at 1224 cm^{-1}. Figure 11, which presents the conversion rate α as a function of irradiation time, gives a qualitative description of the carbazolyl radical formation.

A comparison of the shapes of the curves given in Figures 10 and 11 suggests a relationship between the degradation of the C−N at 1224 cm^{-1} and an increase in the carbonyl products and the formation of free carbazole. On the basis of the curves given

dx.doi.org/10.1021/jp211358q |J. Phys. Chem. B 2012, 116, 802–812

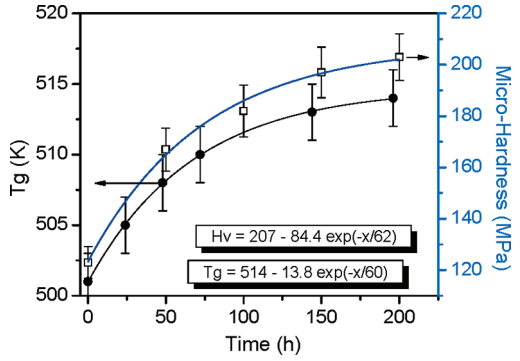

Figure 12. Hv (□) and T_g (●) versus photo-oxidation duration. The lines are the kinetic curves obtained by an exponential fit.

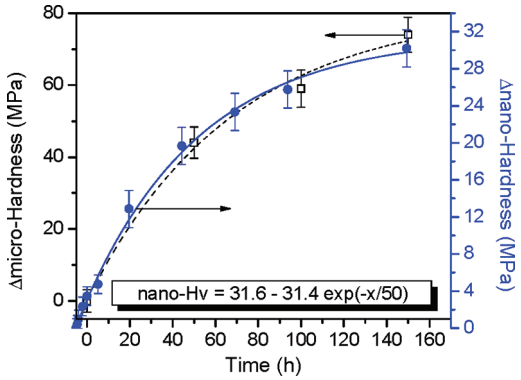

Figure 13. ΔHv (□) and Δnano-H (●) versus photo-oxidation duration. The lines are the kinetic curves obtained by an exponential fit.

in these figures, one can determine the concentrations of the products that were formed. The molar extinction coefficient (ε) of the NH groups was calculated with an IR calibration obtained with several concentrations of molecular carbazole in KBr plates and then compared to other values obtained in the literature. An average value around 90 mol L^{-1} cm^{-1} was evaluated. We used an ε of 340 mol L^{-1} cm^{-1} for the ketone product.[38,39] After 150 h, the concentration of ketone photoproducts in the PVK matrix was calculated as 9.10^{-4} mol L^{-1} and the amount of free carbazole as 6.10^{-4} mol L^{-1}. These results show that these photoproducts are formed in the same order of concentration, which gives a confirmation of a direct correlation between the two photoproducts.

3.B.2. Modifications of the Physical Properties As Measured by m-H, DSC, and AFM. ***a. Analysis of Bulk and Surface.*** Measurement of the Vickers Hv versus exposure time (Figure 12) showed a marked increase in Hv in the first 10 μm. One can observe that the evolution of the Hv with the aging time presents the same trend as the IR band that characterized the modifications of the chemical structure (see Figure 10). This reflects the direct correlation between the modifications of both the chemical structure and the physical properties.

On the basis of these results, we investigated the network densification in the polymer bulk by DSC. The consequences of photo-oxidation were first monitored by DSC with respect to the glass transition temperature (T_g) as reported in Figure 12. We observed a shift in the T_g to a higher temperature. It is well-known that the glass transition temperature of a polymer is related to the cross-link density.[40,41] The predominant phenomenon in photo-oxidation is an increase in the cross-link density, which is highlighted by this shift in the T_g. The evolution of this property in the bulk upon aging was consistent with the densification of the network revealed by Hv measurements.

These observations are in total agreement with our previous results.[1] It was observed that M_w increased versus irradiation time, which confirmed that cross-linking reactions took place during photo-oxidation. This phenomenon is described by eq 10,[40] which indicates that an increase in the M_w resulting from cross-linking can provoke an increase in the T_g

$$T_g = T_{g(linear\infty)} - K/M_w \qquad (10)$$

where K is a factor depending on the free-volume evolution and M_w is the molecular weight.

The modifications of the polymer surface were investigated by AFM nanoindentations. Figure 13 compares the variation of

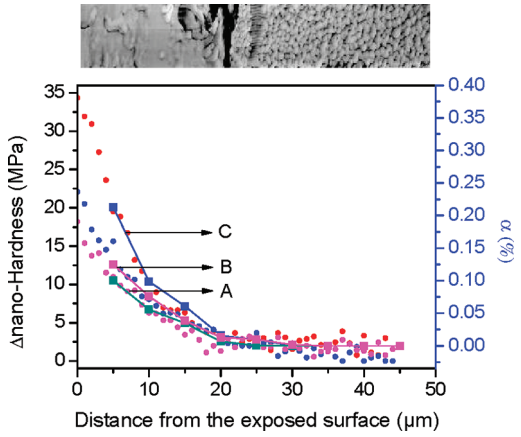

Figure 14. Bottom: Δnano-H (●) and conversion rate of the CN groups at 1224 cm^{-1} (■) versus thickness (μm). Trace A, t = 50 h; trace B, t = 100 h; trace C, t = 200 h. Top: image of the irradiated PVK samples (right) embedded in an epoxy resin.

Δnano-H as a function of irradiation time, with the variations of Hv.

One can observe a good agreement in terms of the trend between the values given by Hv and those calculated from the AFM indentation measurements, though the obtained values were quite different. The differences between the two sets of data that were monitored can be explained by the shape of the oxidation profile, the sample used for Hv measurements (i.e., PVK deposited on an iron plate) and by the inherent error of the mathematical model.[42,43] However, these sets of data definitely confirmed the network densification, even at the extreme surface of the polymer. In conclusion, whatever the investigated scale, our results clearly indicate that the cross-link density increased as a function of irradiation duration.

b. Characterization of the Profiles. To evaluate the cross-link rate within the thickness of the irradiated films, depth-profile experiments were realized by AFM in nanoindentation mode. The stiffness profiles were obtained for thick polymer films of PVK (~100 μm), and nanoindentation curves were recorded every micrometer (Figure 14). Figure 14 also shows the depth profiling by IR microspectroscopy that characterizes the distribution of C−N scissions.

The results given in Figure 14 indicate that the degradation is limited to 25 μm, which is similar to the results obtained in the case of irradiation in the absence of oxygen. This confirms the

dx.doi.org/10.1021/jp211358q | J. Phys. Chem. B 2012, 116, 802–812

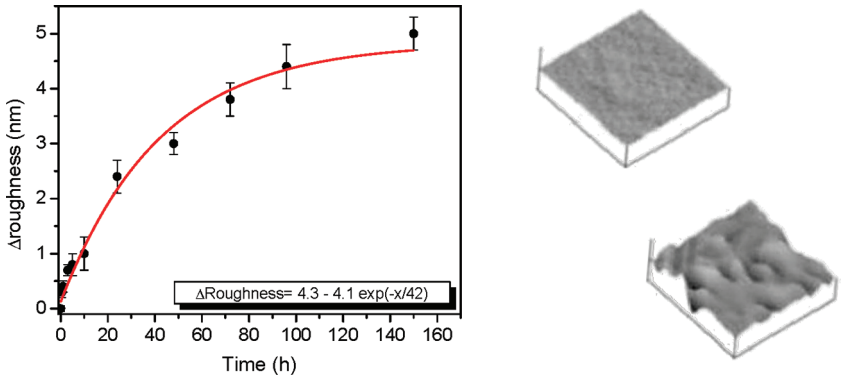

Figure 15. Left: Δroughness (●) versus photo-oxidation duration. The line is a kinetic curve obtained by an exponential fit. Right: image of the PVK surface before and after aging.

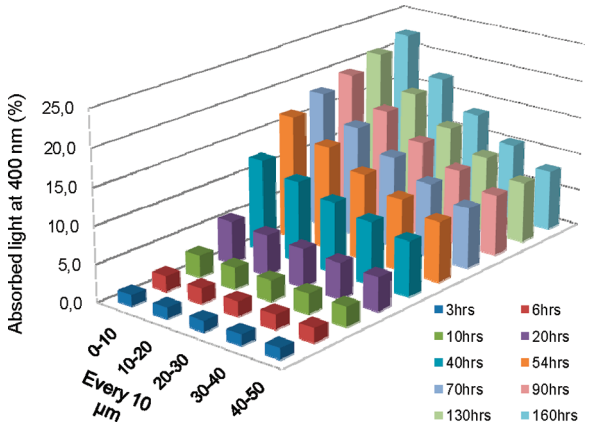

Figure 16. Profile of photoproducts absorption at 400 nm along the depth of the irradiated polymer sample.

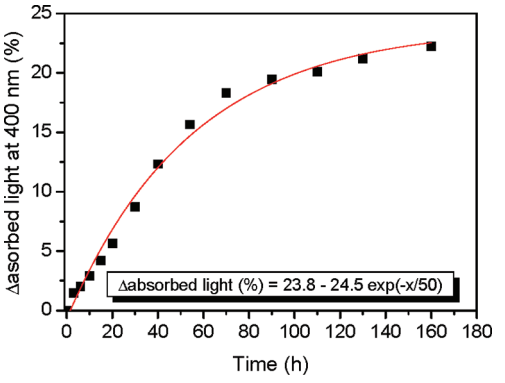

Figure 17. Absorbed light at 400 nm (■) versus photo-oxidation duration. The squares represent the experimental points, and the line is the extrapolated curve obtained by an exponential fit.

previous results showing that the depth of the degradation only depends on the penetration of light into polymer and not on the oxygen permeability.[12] Figure 14 also shows that the increase in stiffness provoked by photo-oxidation is more substantial than that observed in the absence of oxygen. This result suggests that oxygen enhances the cross-linking reactions. The depth-profiling experiments confirm the presence of a steeper cross-linking density and the C−N bond consumption gradient in the thickness of the polymer when irradiation is performed in ambient air. Furthermore, in the presence of oxygen, an increase in stiffness by a factor of 2 can be observed between 50 and 200 h of irradiation. We have previously reported[14] that the average mesh size distribution determined by thermoporosimetry analysis, which characterize the cross-linking density and the concentration of released carbazole groups, was modified at the same rate. These parallel evolutions confirm a direct correlation between the modification of the chemical structure and the evolution of the mechanical properties.

3.B.3. Evolution of the Macroscopic Properties As Measured by UV−Visible Spectroscopy and AFM. Roughness data for PVK samples subjected to photo-oxidation are reported in Figure 15. This figure shows that the rms roughness increased throughout irradiation with a change in the slope and a lower rate after ∼50 h of exposure.

Conversely, the increase in the roughness evolution provoked by irradiation in the absence of oxygen was lower than 1 nm. This weak evolution is related with the cross-linking reaction because no other reaction can occur in these conditions of exposure. The cross-linking rate is approximately 4 times higher in the presence of oxygen, which is in the same order as the gap recorded for the surface roughness. The accumulation of the oxidation products in the polymer sample could account for this phenomenon. Indeed, it has been previously reported that hydroperoxide decomposition, which gives carbonyl products, leads to a roughness increase,[24] and we noticed that the kinetics of the carbonyl product accumulation is similar to the roughness increase (see Figure 10).

The formation of oxidation photoproduct absorption in the visible domain was monitored in the thick films by UV−visible spectroscopy at 400 nm. Using the Beer−Lambert law, it is possible to calculate the accumulation profile of these species within the thickness of the sample. These profiles are reported in Figure 16.

The most important point concerns the first 10 μm of the irradiated sample. Most of the photoproduct absorption at 400 nm (yellowing) is located in these first 10 μm. In Figure 17, the absorbance at 400 nm of this slice of 10 μm was reported as a function of the irradiation time. The shape of the profile follows the same trend as both the accumulation of the oxidative photoproducts and the evolution of roughness. This result clearly indicates that these phenomena are closely correlated.

3.B.4. Mechanism of Degradation. The results given in the former sections indicate a loss of the C−N bond, an increase in the NH band intensity, an increase in the Hv and T_g and an increase in the nano-H are correlated. On the basis of these results and those of previous work, a degradation mechanism can be proposed that accounts for the close relationship between the

dx.doi.org/10.1021/jp211358q |J. Phys. Chem. B 2012, 116, 802–812

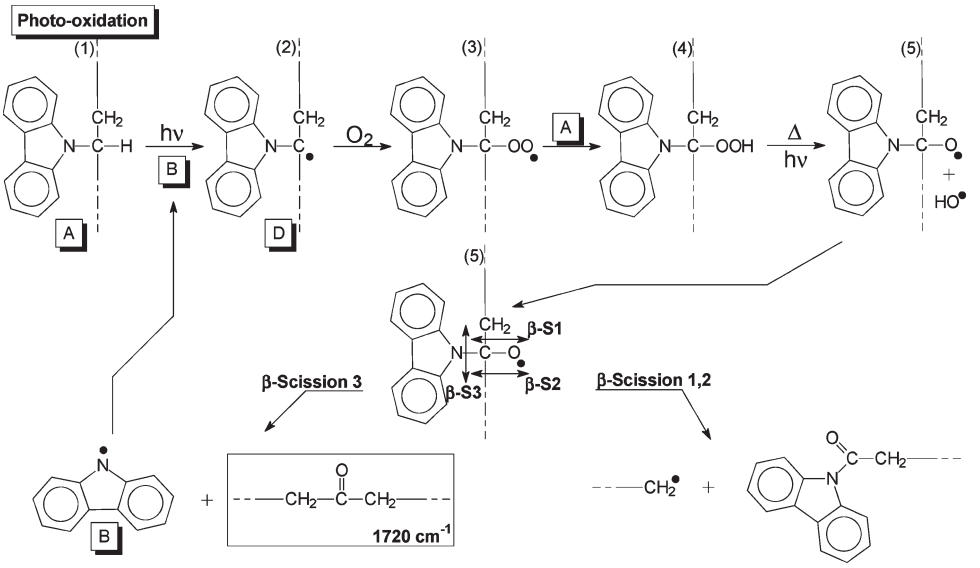

Figure 18. Photo-oxidation mechanism of PVK.

modifications of the chemical structure and the evolution of the mechanical properties of the polymer under light exposure. The proposed mechanism is depicted in Figure 18.

The successive reactions can be described as follows:

(1) → (2): Radical (B) is formed primarily by a direct photochemical reaction, as described above in the case of photolysis.

(2) → (4): Formation of a hydroperoxide by fixation of atmospheric oxygen following a standard oxidation mechanism.[44,45]

(4) → (5): Hydroperoxide decomposition under light and temperature to form an alkoxy radical that can decompose through three possible β-scissions with the formation of different photoproducts.

In a previous paper, we have determined that β-scission 1,2 was the main route of degradation because these reactions can explain the formation of all the major oxidation photoproducts and thus give a complete mapping of the PVK degradation.

The results given in this article show that cross-linking is the main route of evolution of PVK in conditions of photo-oxidation. Reactions following β-scission 3 show a direct relationship between the formation of a ketone at 1720 cm^{-1}, the formation of molecular carbazole (B) and a tertiary macroradical, and the polycarbazolyl radical (D), which might recombine, leading to cross-linking. β-scission 3 can then be reconsidered as the major route that accounts for the cross-linking reaction. Furthermore, it is important to note that the carbazolyl radical (B) (which is the initiator of the mechanism but also produced by the β-scission 3) gives a closed-loop mechanism that can explain the good agreement between all the measured parameters and the predominance of the cross-linking reactions.

C. Calculation of Correlation Factors. We have shown above that the degradation of PVK leads to modifications of

- the chemical structure (oxidation and cross-linking)
- the macromolecular architecture (increase in the network density, i.e., T_g)
- the mechanical properties (increase in the hardness)
- the functional properties (increase in roughness and yellowing).

Cross-linking, network density increase and hardness increase are relevant in terms of a loss of the material functional properties because photo-oxidation of PVK results in unacceptable crack formation, substantial yellowing and a roughness increase.[24,46−48] Therefore, the degradation caused by exposure to UV radiation can be characterized by the following parameters: C−N conversion rate, an increase in the NH band intensity, T_g, nanoindentation and Hv increase. To verify the correlation between the evolution of these parameters during irradiation, a quantitative description was attempted.

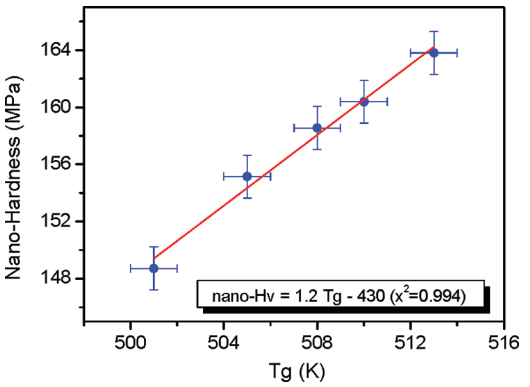

Figure 19. Nano-H values versus T_g (circles); temperatures are in Kelvin.

Table 3. $-B/A$ Ratio Calculated from eq 11 and Derived from Other Work[37] and Our Measurements

origins	ratio $-B/A$ (K)	correlation coeff., x^2	ref
Batholomeo et al.	308	0.99	37
nano-Hv = $f(T_g)$	358 ± 20	0.99	

We first tried to establish the quantitative relationship between nano-H and T_g on the basis of eq 11.

$$\mathrm{Hv} = AT_g + B \tag{11}$$

This equation has been proposed by Fakirov et al.,[49] where A and B are two empirical coefficients, Hv is measured at T_{amb}, and

dx.doi.org/10.1021/jp211358q | J. Phys. Chem. B 2012, 116, 802–812

Table 4. Degradation Rate k for the Main Degradation Criteria in the PVK Photodegradation

parameters	k ($h^{-1} \times 10^{-2}$)	standard error ($h^{-1} \times 10^{-2}$)	correlation coeff., x^2
Irradiation in the Presence of Oxygen			
α - CN	2.4	±0.05	0.997
Abs − C═O	2.7	±0.15	0.995
Abs - NH	2.9	±0.2	0. 994
Hv	1.6	±0.25	0.962
nano-Hv	2	±0.15	0.981
T_g	1.7	±0.05	0.99
roughness (nm)	2.4	±0.5	0.963
yellowing	2	±0.2	0.989
Irradiation in the Absence of Oxygen			
α - CN	1.05	±0.1	0.991
Abs - NH	1.0	±0.15	0. 987
nano-Hv	1.1	±0.2	0.985

the T_g value is between T_{amb} and T = 523 K. Fakirov et al. applied this relationship to different polymers. In our case, we tried to validate this law in the case of PVK, whose mechanical properties are changed as a consequence of photoaging. The results are reported in Figure 19.

Table 3 gives the calculated ratio of $-B/A$ for the relationship between nano-H vs T_g and for another value derived from the work published by Bartholomeo et al.[50]

A linear law was obtained for nano-H versus T_g, with a ratio $(-B/A)$ close to that obtained by Fakirov et al.[49] This result highlights the direct relationship between the modifications of macromolecular architecture (T_g) and those of mechanical properties (hardness).

To connect all of the degradation criteria from the microscopic scale to the macroscopic scale, we searched for kinetic information in the different parameters responsible for the degradation versus exposure time. We used a phenomenological model[51,52] to describe the kinetic processes of degradation in the form of eq 12.

$$\frac{dX}{dt} = Ae^{-E_a/RT}(X_\infty - X)^n \quad (12)$$

Equation 12 is only meaningful for discrete values of n.[53] For n = 1, integration of eq 12 gives relation 13

$$X = X + (X_0 - X_\infty)e^{-kt} \quad (13)$$

where X_∞ is the parameter value obtained for $t \rightarrow \infty$, X_0 is the parameter value at t = 0, and k is the Arrhenius-type kinetic constant. The equation was applied to experimental parameters X (α CN, abs NH, abs CO, T_g, nano-H, roughness, and yellowing) for different values of n. The best fits were achieved with a first-order model (n = 1), which perfectly fits the experimental data, as shown in Figures 4, 6, 9−12, 15, and 17. A first-order reaction mechanism can be described by a negative exponential function between concentration and time. Postulating that the X parameter allows the product concentration to be measured, the results indicated that the determining step in the degradation mechanism under UV irradiation had a first-order rate, with a degradation rate k given by eq 13. The use of first-order rate kinetics is even more tangible because the photo-oxidation and photolysis processes are only governed by absorbed light with no limitation on the O_2 diffusion, as explained before (cf. Figure 14).

The k values obtained considering the different measured parameters X, which account for the degradation of PVK, are reported in Table 4.

All of these parameters follow the same exposure time dependence, and the k (degradation rate) values for the main parameters are very close. The good agreement between the degradation rates k of the different criteria confirmed that the degradation of the functional properties can be correlated to the modifications of the chemical structure. The half-life time was calculated from the kinetics, with an average k value of 2.2×10^{-2} h^{-1} and an average $t_{1/2}$ value of 32 h in the presence of oxygen and an average k value of 1.05×10^{-2} h^{-1} and an average $t_{1/2}$ value of 70 h in the absence of oxygen.

4. CONCLUSIONS

In this paper, we analyzed the consequences of photoaging on PVK in the presence and in the absence of oxygen. We realized depth-profiling experiments and roughness and stiffness measurements by AFM in combination with the use of other techniques, such as gel fraction, SEC, Hv, and infrared analysis.

Results confirmed that the cross-linking reactions are predominant in photodegradation and that the degradation is governed by the penetration of light. It has been shown that cross-linking results in the formation of a three-dimensional network, which provokes an increase in stiffness that can be measured at the surface of the irradiated film. The influence of oxygen on the cross-linking rate has been determined, and it has been shown that oxygen enhances cross-linking events. The most outstanding result obtained is the quantitative correlation between the modifications of the chemical structure and the variation of the physical properties at each scale of analysis.

AUTHOR INFORMATION

Corresponding Author

*E-mail: p-olivier.bussiere@univ-bpclermont.fr. Phone: +33(4) 73 40 55 18. Fax: +33(4) 73 40 77 00.

ACKNOWLEDGMENT

This work was supported by the "Conseil Regional d'Auvergne" under a grant named "Projet Jeune Chercheur".

REFERENCES

(1) Sariciftci, N. S.; Smilowitz, L.; Heeger, A. J.; Wudl, F. *Science* **1992**, *258*, 1474–1476.
(2) Dennler, G.; Scharber, M. C.; Brabec, C. J. *Adv. Mater.* **2009**, *21*, 1323–1338.
(3) Heeger, A. *J. Chem. Soc. Rev.* **2010**, *39*, 2354–2371.
(4) Yang, X.; Loos, J. *Macromolecules* **2007**, *40*, 1353–1362.
(5) Chen, L.-M.; Hong, Z.; Li, G.; Yang, Y. *Adv. Mater.* **2009**, *21*, 1434–1449.
(6) Thompson, B. C.; Frechet, J. M. J. *Angew. Chem.Int. Ed.* **2008**, *47*, 58–77.
(7) Kippelen, B.; Bredas, J. L. *Energ. Environ. Sci.* **2009**, *2*, 251–261.
(8) Bundgaard, E.; Krebs, F. C. *Sol. Energy Mater. Sol. Cell.* **2007**, *91*, 954–985.
(9) (a) Blouin, N.; Michaud, A.; Leclerc, M. *Adv. Mater.* **2007**, *19*, 2295–2300. (b) Blouin, N.; Michaud, A.; Gendron, D.; Wakim, S.; Blair, E.; Neagu-Plesu, R.; Belletete, M.; Durocher, G.; Tao, Y.; Leclerc, M. *J. Am. Chem. Soc.* **2008**, *130*, 732–742.

(10) (a) Jorgensen, M.; Norrman, K.; Krebs, F. C. *Sol. Energy Mater. Sol. Cell.* **2008**, *92*, 686–714. (b) Manceau, M.; Bundgaard, E.; Carlé, E. J.; Hagemann, O.; Helgesen, M.; Sondergaard, R.; Jorgensen, M.; Krebs, F. C. *J. Mater. Chem.* **2011**, *21*, 4132–4141.
(11) Cho, S.; Seo, J. H.; Park, S. H.; Beaupré, S.; Leclerc, M.; Heeger, A. J. *Adv. Mater.* **2010**, *22*, 1253–1257.
(12) Rivaton, A.; Mailhot, B.; Derderian, G.; Bussiere, P. O.; Gardette, J. L. *Macromolecules* **2003**, *36*, 5815–5824.
(13) Pfister, G.; Williams, D. J. *J. Chem. Phys.* **1974**, *61*, 2416–2426.
(14) Bussière, P. O.; Mailhot, B.; Rivaton, A.; Barthe, M. F.; Gardette, J. L.; Baba, M. *Polym. Degrad. Stab.* **2008**, *93*, 1376–1382.
(15) Lucas, P.; Baba, M.; Lacoste, J.; Gardette, J.-L. *Polym. Degrad. Stab.* **2002**, *76*, 449–453.
(16) Kelen, T. *Polymer Degradation*; Van Nostrand: New York, 1983.
(17) Musto, P. *Macromolecules* **2003**, *36*, 3210–3221.
(18) English, A. D.; Chase, D. B.; Spinelli, H. J. *Macromolecules* **1983**, *16*, 1422–1427.
(19) Carter, R. O., III; Paputa Peck, M. C.; Bauer, D. R. *Polym. Degrad. Stab.* **1989**, *23*, 121–134.
(20) Malajati, Y.; Therias, S.; Gardette, J.-L. *Polym. Degrad. Stab.* **2011**, *96*, 144–150.
(21) Paci, B.; Generosi, A.; Bailo, D.; Rossi Albertini, V.; de Bettignies, R. *Chem. Phys. Lett.* **2010**, *494*, 69–74.
(22) Eleni, P. N.; Krokida, M. K.; Polyzoi,s, G. L.; Charitidis, C. A.; Koumoulos, E. P.; Tsikourkitoudi, V. P.; Ziomas, I. *Polym. Degrad. Stab.* **2011**, *96*, 470–476.
(23) Mailhot, B.; Morlat-Thérias, S.; Bussière, P.-O.; Le Pluart, L.; Duchet, J.; Sautereau, H.; Gérard, J.-F.; Gardette, J.-L. *Polym. Degrad. Stab.* **2008**, *93*, 1786–1792.
(24) Mailhot, B.; Morlat-Thérias, S.; Gardette, J.-L. *Polymer* **2000**, *41*, 1981–1988.
(25) Mailhot, B.; Bussière, P.-O.; Rivaton, A.; Morlat-Thérias, S.; Gardette, J.-L. *Macromol. Rapid Commun.* **2004**, *25*, 436–440.
(26) Lemaire, J.; Arnaud, R.; Gardette, J. L. *Rev. Gen. Caoutchouc Plast.* **1981**, *613*, 87.
(27) Herbert, E. G.; Pharr, G. M.; Oliver, W. C.; Lucas, B. N.; Hay, J. L. *Thin Solid Films* **2001**, *398*−*399*, 331–335.
(28) Cappella, B.; Kaliappan, S. K.; Sturm, H. *Macromolecules* **2005**, *38*, 1874–1881.
(29) Reynaud, C.; Sommer, F.; Quet, C.; Bounia, N. E.; Tran Minh, D. *Surf. Interface Anal.* **2000**, *30*, 185–189.
(30) Oliver, W. C.; Pharr, G. M. *J. Mater. Res.* **1992**, *7*, 1564–1583.
(31) Jee, A.-Y.; Lee, M. *Polym. Test.* **2010**, *29*, 95–99.
(32) Sneddon, I. N. *Int. J. Engng. Sci.* **1965**, *3*, 47–57.
(33) Bhushan, B. In *Handbook of Micro/Nano Tribology*; Bhushan, B., Ed.; CRC Press: Boca Raton, FL, 1995; p 321.
(34) Touhami, A.; Nysten, B.; Dufrêne, Y. F. *Langmuir* **2003**, *19*, 4539–4543.
(35) Finke, M.; Hughes, J. A.; Parker, D. M.; Jandt, K. D. *Surf. Sci.* **2001**, *491*, 456–467.
(36) Butt, H. J.; Cappella, B.; Kappl, M. *Surf. Sci. Rep.* **2005**, *59*, 1–152.
(37) Rivaton, A.; Mailhot, B.; Robu, S.; Lounaci, M.; Bussière, P.-O; Gardette, J.-L. *Polym. Degrad. Stab.* **2006**, *91*, 565–572.
(38) Nakanishi, K., *Infrared Absorption Spectroscopy*; Holden Day: San Francisco, CA, 1962.
(39) Ivan, G.; Giurginca, M. *Polym. Degrad. Stab.* **1998**, *62*, 441–446.
(40) Fox, T. G.; Loshaek, S. *J. Polym. Sci.* **1955**, *15*, 371–390.
(41) Bicerano, J.; Sammler, R. L.; Carriere, C. J.; Seitz, J. T. *J. Polym. Sci., Polym. Phys.* **1996**, *34*, 2247–2259.
(42) Tranchida, D.; Piccarolo, S.; Soliman, M. *Macromolecules* **2006**, *39*, 4547–4546.
(43) Perrin, F. X.; Nguyen, V.; Vernet, J. L. *Polymer* **2002**, *43*, 6159–6167.
(44) Carduner, K. R.; Carter, R. O.; Zinbo, M.; Gerlock, J. L.; Bauer, D. R. *Macromolecules* **1988**, *21*, 1598–1603.
(45) Wilhelm, C.; Gardette, J.-L. *Polymer* **1998**, *39*, 5973–5980.
(46) Larché, J.-F.; Bussière, P.-O.; Gardette, J.-L. *Polym. Degrad. Stab.* **2010**, *95*, 1810–1817.
(47) Larché, J.-F.; Bussière, P.-O.; Gardette, J.-L. *Polym. Degrad. Stab.* **2011**, *96*, 1530–1536.
(48) Nichols, M. E.; Darr, C. A. *Service Life Prediction of Organic Coatings*; American Chemical Society: Washington, DC, 1999; Vol. 722, pp 332−353.
(49) Fakirov, S.; Baltá Calleja, F. J.; Krumova, M. *J. Polym. Sci., Polym. Phys.* **1999**, *37*, 1413–1419.
(50) Bartolomeo, P.; Irigoyen, M.; Aragon, E.; Frizzi, M. A.; Perrin, F. X. *Polym. Degrad. Stab.* **2001**, *72*, 63–68.
(51) Šimon, P.; Cibulková, Z.; Thomas, P. *J. Therm. Anal. Calorim.* **2005**, *80*, 381–385.
(52) Musto, P.; Ragosta, G.; Abbate, M.; Scarinzi, G. *Macromolecules* **2008**, *41*, 5729–5743.
(53) Rose, N.; Le Bras, M.; Bourbigot, S.; Delobel, R. *Polym. Degrad. Stab.* **1994**, *45*, 387–397.